Carbon 139 (2018) 759–767

Contents lists available at ScienceDirect

Carbon

journal homepage: www.elsevier.com/locate/carbon

Designed fabrication of reduced graphene oxides/Ni hybrids for effective electromagnetic absorption and shielding

Wei Xu, Guang-Sheng Wang*, Peng-Gang Yin

Key Laboratory of Bio-Inspired Smart Interfacial Science and Technology of Ministry of Education, School of Chemistry, Beihang University, Beijing, 100191, PR China

ARTICLE INFO

Article history:
Received 12 April 2018
Received in revised form
20 June 2018
Accepted 20 July 2018
Available online 23 July 2018

ABSTRACT

Reduced graphene oxide (rGO)/Ni hybrids with different mass ratio are successful synthesized in order to tune the microwave absorption together with the electromagnetic shielding performance. By properly adjusting the permittivity and permeability derived from different contents of the rGO and Ni, an rGO/Ni composite with excellent microwave absorption properties is obtained. An optimal reflection loss value of −39.03 dB at 13 GHz is achieved for the composite with rGO/Ni ratio of 1:1, and the bandwidth less than −10 dB can reach up to 4.3 GHz (from 11 to 15.3 GHz) with a thickness of 2.0 mm. Furthermore, the composite with rGO/Ni ratio of 4:1 shows superior electromagnetic shielding performance as high as 52 dB, which far surpasses the best value for most carbon-based materials. Fundamental mechanisms for absorbing and shielding performance are discussed.

1. Introduction

In the modern era, with the rapid development of the electronics industry and extensive use of communication devices, electromagnetic pollution has become a quite serious and widespread problem. The materials of electromagnetic (EM) radiation absorbing and electromagnetic interference (EMI) shielding have attracted much attention owing to their significant role either in attenuating those unwanted EM energies or acting as a shield against the penetration of the undesirable EM irradiation [1–3]. It is well recognized that both the absorption property and the EMI shielding performance of materials are directly determined by their permittivity, permeability, as well as matching condition; while these features are profoundly dependent on the dielectric property, magnetism, and conductivity [4,5]. Recently, many researchers have proved that materials with only one single composition were unable to meet the requirement of impedance matching thus leading to severe issues such as high functional filler loading, thick coating thickness, and narrow effective bandwidth [6]. Accordingly, incorporation of dielectric loss materials with magnetic loss materials should be an ideal method to achieve effective regulation of electromagnetic parameters [7–9]. For that reason, various composites have been developed to obtain improved performance, such as Ni@SnO_2 [10], NiO/SiC [11], Fe_3O_4/TiO_2 [12], CoNi@Air@TiO_2 [13], MoS_2/rGO [14,15], Fe/CNT [16] and so on.

Among these materials, rGO consisting of a single layer of carbon atoms in a closely honeycomb hexagonally packing, not only possesses a stable tow-dimensional structure and abundant functional groups but also exhibits extremely high specific surface area and excellent electrical conductivity [17–19]. These properties endow rGO with potential applicability to be used as an EM absorber as well as EMI shielding material [20,21]. However, as a nonmagnetic material, rGO can only induce a strong dielectric loss thus leading to a relatively poor performance [22]. One feasible approach to overcome this drawback is to combine magnetic compositions with rGO, which can not only integrate the advantages of the individual components but also control the electromagnetic parameters of materials. Zong et al. [23] synthesized rGO/Fe_3O_4 composites by a rational one-pot simplified co-precipitation route, which exhibited strong reflection loss (RL) was up to −44.6 dB at 6.6 GHz with 50 wt% of rGO/Fe_3O_4 being used in wax, while a thickness of 3.9 mm was demanded. Zhang et al. [14] reported a single-mode microwave-assisted hydrothermal method to fabricate CoS_2/rGO nanohybrids, and the minimum RL of −56.9 dB was achieved with the thickness of 2.2 mm. On the other hand, a great deal of research is being focused on EMI shielding materials with rGO-based hybrids. For example, Mishra et al. [24] investigated that the conducting ferrofluid composites with rGO/Fe_3O_4

* Corresponding author.
E-mail address: wanggsh@buaa.edu.cn (G.-S. Wang).

https://doi.org/10.1016/j.carbon.2018.07.044
0008-6223/

possessed high shielding effectiveness (SET ~41 dB), resulting from the combined effect of magnetic losses and rGO. Similarly, Singh [25] developed Fe_3O_4/rGO/polyaniline composites by the in-situ generation, and the resultant structures exhibited good electrical conductivity (as high as 2.6 S cm^{-1}) with an EMI shielding of ~36 dB when the composite thickness was 2.5 mm.

In fact, a moderate conducting material is suitable as an EM absorbing material, whereas material with high conductivity make it a promising candidate as an EMI shield [26]. Meanwhile, too high permittivity can hardly satisfy an ideal absorber but favors to EMI shielding [27]. In this context, varying the ratio of rGO and the magnetic composition is an efficient method to achieve permittivity regulation so that the properties of composites can be tailored for desired effects, namely, for highly EM wave-absorbing property, a good balance between permittivity and permeability is in urgent need; while for achieving effective EMI shielding, higher permittivity is favorable. Unfortunately, there have been few reports on the aforementioned properties. Herein, a large scale of Ni chains has been synthesized and evenly embedded in the rGO nanosheets with different proportions. The properties of resultant composites can be artificially controlled by regulating the combination ratio. A remarkable reflection loss of approximately −40 dB and a superior EMI shielding effectiveness (SE) over 52 dB are achieved by tailoring the proportion of rGO and Ni to a certain ratio of 1:1 and 4:1, respectively, which confirms that the composites have excellent EM absorbing as well as EMI shielding properties. In addition, we have further investigated the corresponding mechanism, relationship and difference between EM absorbing and EMI shielding properties based on complex permittivity, impedance matching condition and conductivity.

2. Experimental

2.1. Materials

Graphene Oxide (GO) was synthesized from graphite powder according to a modified Hummer's method. Other chemicals and reagents were purchased from Beijing Chemicals Factory. Deionized water was used in all experiments.

2.2. Fabrication of the Ni nanochains and the rGO/Ni nanohybrids

Ni nanochains were prepared according to our previous work [28]. In brief, 0.119 g of $NiCl_2 \cdot 6H_2O$ and 0.333 g of polyvinyl pyrrolidone were dissolved in 100 ml of ethylene glycol (EG) solvent with mechanical stirring for 2 h to obtain a transparent solution. Next, 0.265 mL of the hydrazine monohydrate liquid (80%) was added to the as prepared solution dropwise. After stirring for 2 h, the homogeneous suspension was transferred to a heating jacket and heated to the boiling point of EG (~197 °C) with refluxing for 3 h, then a dark precipitate was obtained. Subsequently, the precipitate was washed several times with distilled water and absolute ethanol and finally dried at 60 °C for 12 h for further characterization.

The rGO/Ni nanohybrids were synthesized by a facile synthetic route. First, the graphene oxides with different mass were put in deionized water with ultrasonic treatment for 2 h to obtain a homogeneous dispersion. Then this solution was heated to 90 °C in an oil bath under magnetic stirring, after that, a certain amount of $N_2H_4 \cdot H_2O$ was dissolved in the reaction solution. After stirring for 3 h, the solution was cooled to room temperature and then the as-synthesized Ni chains were added in, with continuing sonicating for another 2 h. Finally, the black mixture was collected by centrifugation and washed several times using the deionized water and then freeze-dried at −50 °C for 48 h to get rGO/Ni hybrids powders. The mass ratio between rGO and Ni were 4:1, 2:1, 1:1, 1:2, and 1:4, respectively.

2.3. EM absorption and EMI shielding measurement

The composites used for EM absorption and shielding measurement were prepared by mixing the hybrids with poly(-vinylidene fluoride) PVDF in 10 wt% loading. Afterwards, a cylindrical shaped sample ($\Phi_{out} = 7.00$ mm and $\Phi_{in} = 3.04$ mm) was fabricated by hot-pressing the mixtures in molds. The EM parameters were measured using two-port vector network analyzer (Agilent E5071C) over the frequency of 2–18 GHz, coupled with a coaxial wire setup.

2.4. Characterization

Powder diffraction data of the as-synthesized samples were collected using a Rigaku Dmax 2200 X-ray diffractometer with Cu Kα radiation ($\lambda = 1.5416$ Å) for phase analysis. The morphologies and sizes of samples were examined by scanning electron microscopy (SEM, JEOL JSM-7001F), field emission scanning electron microscopy (FE-SEM, JSM-6700F) and transmission electron microscopy (TEM, JEOL JEM-2010). The elemental composition was detected by energy dispersive spectrometer (EDS) spectrum deriving from the FE-SEM, coupled with copper grids. Raman spectra were measured using a LabRAM HR800 Laser Raman spectroscopy (HORIBA Jobin Yvon CO. Ltd., France) by using a 632.5 nm argon ion laser. Fourier transform infrared spectra (FT-IR) were recorded on a Nicolet IR 200 FT-IR spectrometer (Thermo Scientific) in transmission mode. Magnetic properties of the samples were measured at room temperature by a Lakeshore Vibrating Sample Magnetometer (VSM, Riken Denshi Co. Ltd, Japan).

3. Results and discussion

The phase composition of pure GO and the as-synthesized rGO/Ni were characterized by the X-ray powder diffraction (XRD) and the patterns are presented in Fig. 1a. A diffraction peak around 11.5° in the pure GO is indexed to the (002) plane of graphite oxide. After chemical reduction and decoration, the peak of GO disappears and the broad peak at $2\theta = 23.2°$ corresponding to rGO appears, which could be ascribed to the graphitic structure (002) of the short-range order in stacked rGO sheets [29]. Meanwhile, the peaks at $2\theta = 44.6°$, 51.9°, and 76.5° corresponding to the (111), (200), and (220) planes of face-centered cubic (fcc) Ni crystals (JCPDS no. 04–0850) are observed for the rGO/Ni hybrids, indicating that Ni chains are efficiently assembled on the surface of rGO [28]. Raman spectra exhibit two regular peaks, corresponding to the G band (~1582 cm^{-1}) and D band (~1330 cm^{-1}). Here, the G-band represents the stretching vibration mode in the sp^2-hybridized carbon-carbon bonds, while the D band corresponds to the first-order zone boundary phonon mode associated with defects or lattice distortion [30]. Thus, the intensity ratio of D band to G band (I_D/I_G) provides a sensitive measure of the disorder of the graphitic layers. From Fig. 1b, a major change in the I_D/I_G ratio is observed in the Raman spectra and it is found that the I_D/I_G for as-produced rGO/Ni (1.15) is higher than that of GO (1.04), suggesting a higher degree of defects in the rGO/Ni or the edges due to the reduction process and introduction of the Ni. These defects play an important role in microwave absorbing and shielding.

Fig. 1c shows the normalized FT-IR spectrum of the pure GO and rGO/Ni hybrids. For pure GO, the broad peak around 3300 cm^{-1} is assigned to O–H stretching vibrations of carboxyl groups and the residual water molecules. The characteristic peak appears at 1730, 1634, 1399, and 1085 cm^{-1} indicate the C=O stretching vibration

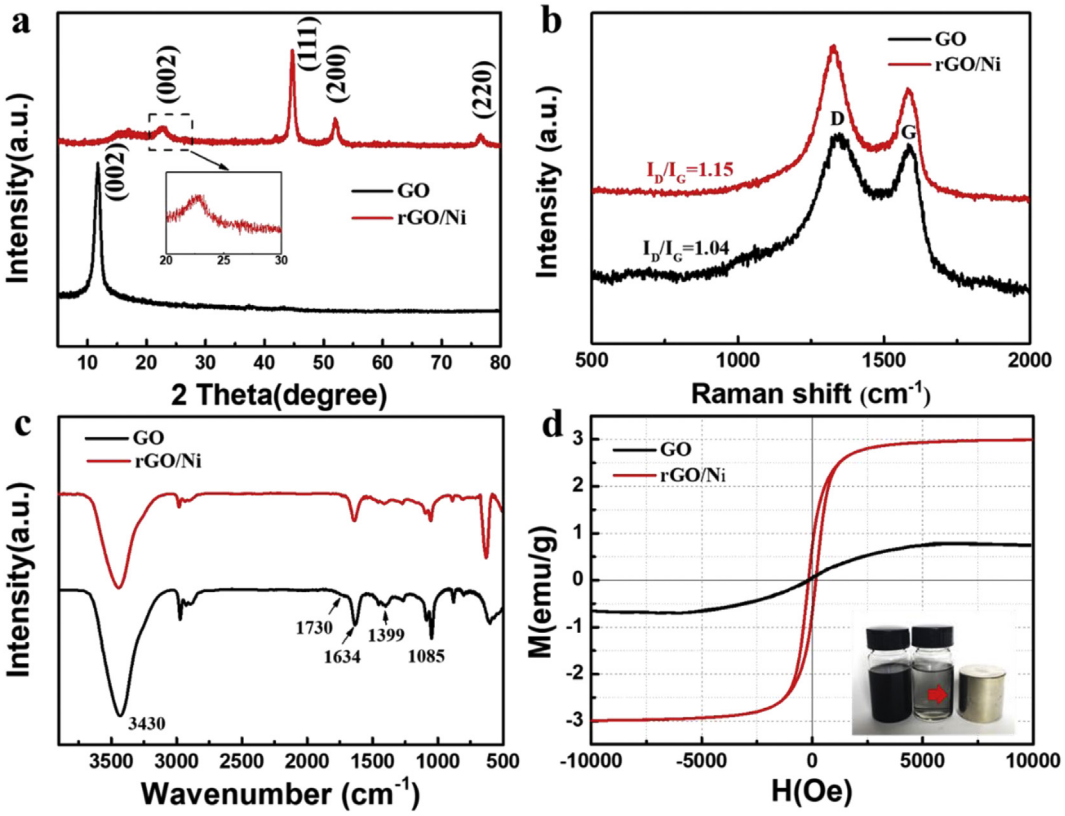

Fig. 1. XRD patterns (a), Raman spectra (b), FTIR spectra (c) and magnetic hysteresis loops (d) of GO and rGO/Ni hybrids in the mass ratio of rGO/Ni to be 1:1. (A colour version of this figure can be viewed online.)

from carbonyl groups, the C=C skeletal stretching vibration from the aromatic carbon, the carboxy C–OH stretching vibration, and the epoxy C–O stretching vibration, respectively [29]. After the chemical reduction at 90 °C, it is evident that the absence of oxygen-containing functional groups and the reduction of hydroxyl peak on the FT-IR spectra of rGO/Ni, implying the partial reduction of GO. The hydroxyl peak did not disappear completely when reduction with hydrazine at a relatively low temperature; its signals disappeared only when the rGO/Ni hybrid was incorporated to PVDF matrix to form composite through a hot-press process at 200 °C, as revealed in Figure S1. In addition, there are four major peaks between 1500 and 750 cm^{-1} that belong to PVDF. Fig. 1d shows the field dependence of magnetization for the GO and rGO/Ni. The M-H curves display a similar S-type shape of GO indicating the paramagnetic behavior with no coercivity and remanence, while a significant hysteresis loop of rGO/Ni suggests the ferromagnetic behavior with a saturating reversible magnetization at room temperature. The inset indicates that when dispersed in ethanol, the nanohybrids would quickly move along the magnetic field.

To investigate the microstructure and morphology of Ni and rGO/Ni nanohybrids, the SEM and TEM of samples were conducted. SEM observations of Ni in Fig. 2a and b shows that the nickel microspheres contact to each other tightly to form chains and their outer diameter and length are approximately 30 nm and 100 μm, respectively. The nano size and magnetism result in the agglomeration. From the TEM images (Fig. 2c and d), both the nearly transparent sheet-like rGO and the dark Ni chains can be found in the hybrids. Moreover, large-scale chains were embedded in or covered by rGO sheets which favor to prevent nickel chains from extensively agglomerating, seen in Fig. 3, the corresponding elemental mapping analysis also suggests that the elemental dispersion of both Ni and C atoms across the system are uniform. Besides, the cross-section SEM image (Figure S2) shows clear nickel chains in the composites, indicating that the Ni can still keep its primary shape after the hot-press procedure.

The complex permittivity ($\varepsilon_r = \varepsilon' - j\varepsilon''$) and complex permeability ($\mu_r = \mu' - j\mu''$) of composites with different mass ratio of rGO/Ni are presented in Fig. 4. The real part (ε') standing for the storage capacity of electric energy is mainly associated with the amount of polarization. Essentially, there are four kinds of mechanisms in polarization which account for the dielectric performance of material, that is, electronic, ionic, orientational and space charge polarization. In a heterogeneous system formed with polarized polymer matrix, orientational and space charge polarization (belonging to relaxation response) play a dominant role at microwave frequency and the process are accompanied by energy dissipation known as the imaginary permittivity (ε''). On the basis of the Debye theory, ε' and ε'' can be described as [31]:

$$\varepsilon' = \varepsilon_\infty + \frac{\varepsilon_S - \varepsilon_\infty}{1 + \omega^2\tau^2} \quad (1)$$

$$\varepsilon'' = \varepsilon_p'' + \varepsilon_c'' = \frac{\omega\tau(\varepsilon_S - \varepsilon_\infty)}{1 + \omega^2\tau^2} + \frac{\sigma}{\omega\varepsilon_0} \quad (2)$$

where ε_∞, ε_S, and ε_0 are the relative dielectric permittivity, the static permittivity at the high-frequency limit and the dielectric constant in a vacuum, respectively, $\omega = 2\pi f$ is the angular frequency, τ represents polarization relaxation time and σ represents the dc conductivity of the composites.

As revealed in Fig. 4a and b, with increasing ratio of the rGO/Ni

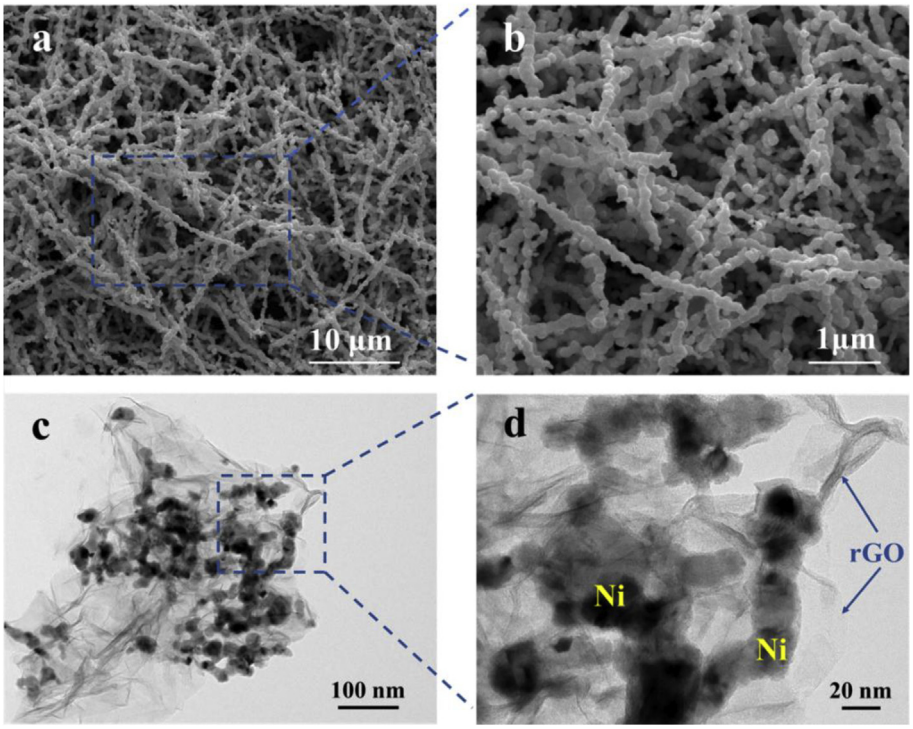

Fig. 2. SEM image (a) and magnified SEM image (b) of Ni chains; TEM image (c) and magnified TEM image (d) of rGO/Ni. (A colour version of this figure can be viewed online.)

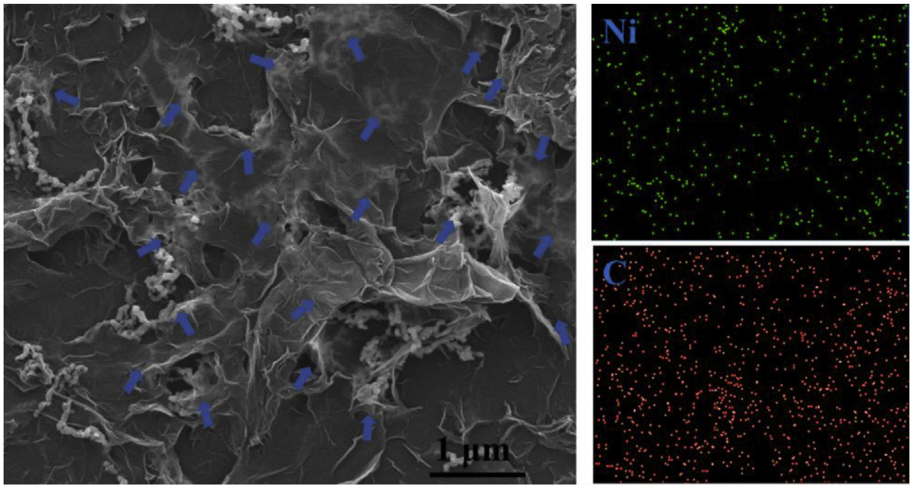

Fig. 3. FESEM image of the rGO/Ni hybrids and corresponding elemental mapping images of Ni and C. (A colour version of this figure can be viewed online.)

from 1:4 to 4:1, the values of ε' increases from 7.7 to 77.8 and ε'' increases from 2.3 to 74 at 2 GHz. The increment of ε' may be attributed to the fact that the rising mass ratio of rGO led to the formation of greater amounts of capacitor-like junctions which contribute to storing the electrical charge at their interfaces and hence cause more space charge polarization. Moreover, the residual functional groups and defects on the surface of rGO generated in the chemical reduction process would induce dipole orientation polarization, which favors for the rising of ε'. On the contrast, the item of ε' decreases with increasing frequency due to the increscent electric leakage that ensues, which is consistent with eq (1).

According to eq (2), the imaginary part ε'' could be regarded as the synergistic contributions of both the conductance loss (ε_c'') and the relaxation loss (ε_p''). That is to say, the dissipation of energy is in the form of the thermal energy generated by relaxation and the Joule heat generated by conductance [32]. The obviously increased ε'' with increasing content of rGO is mainly attributed to the enhancing polarization loss and higher hopping conductivity. When the second part of eq (2) is not taken into account, we obtain,

$$\left(\varepsilon' - \frac{\varepsilon_s + \varepsilon_\infty}{2}\right)^2 + (\varepsilon'')^2 = \left(\frac{\varepsilon_s - \varepsilon_\infty}{2}\right)^2 \quad (3)$$

It corresponds to a semicircle centered at $((\varepsilon_s + \varepsilon_\infty)/2, 0)$, each of which is characteristic for one Debye relaxation process [31]. As shown in Figure S3, the Cole–Cole curve of the composite are distorted due to the synergy effect of multiple polarization mechanisms. Based on the above outcomes, we conclude that the proportion of rGO plays an important role in determining the dielectric behavior of composites. It is worth mentioning that Ni and rGO

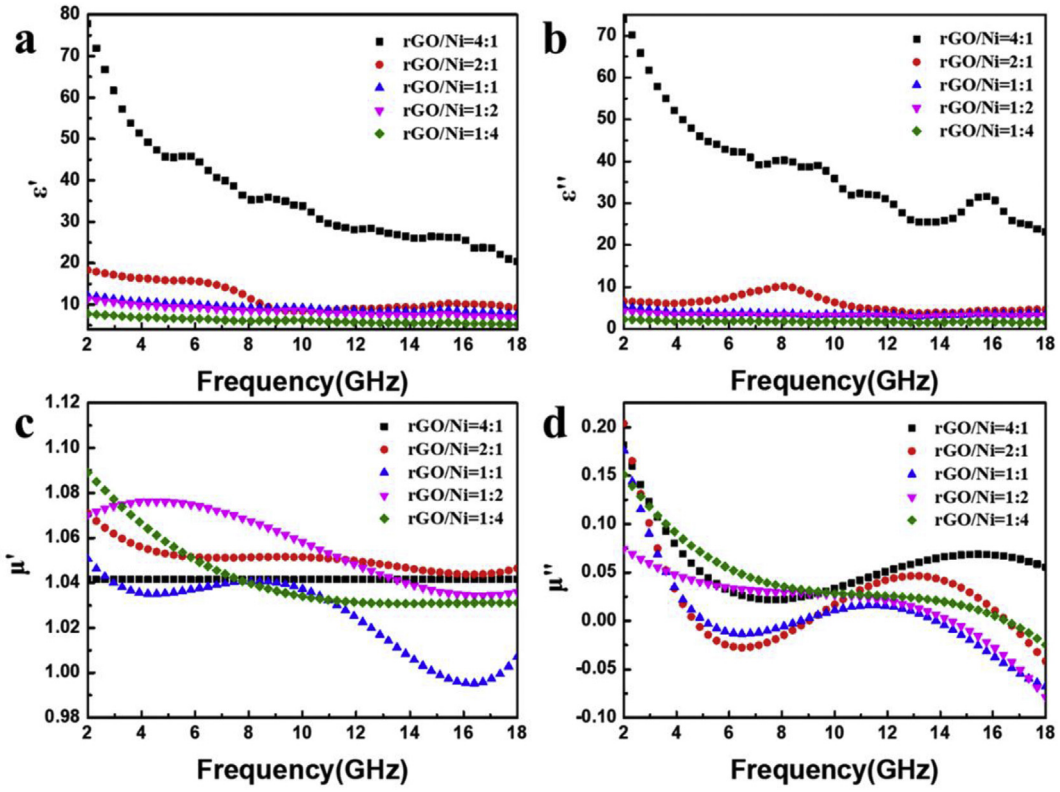

Fig. 4. Frequency dependence of the (a) real part and (b) imaginary part of permittivity, (c) real part and (d) imaginary part of permeability of rGO/Ni hybrids with different rGO proportions. (A colour version of this figure can be viewed online.)

both manifest high electrical conductivity [17,33], but the rGO is folded and has larger specific surface than the chain-like Ni material. Therefore, the rGO link up to form micro-current network easier than the Ni with the same mass ratio, leading to more energy dissipation, which further confirms that the dielectric performance of the nanocomposite originates mainly from rGO.

As for complex permeability, all five samples show similar dispersive behavior with little difference. As shown in the curves of Fig. 4c and d, the μ' and μ'' values of the composites are in the ranges of 0.99–1.08 and (−) 0.08–0.2, respectively. This is because of the nonmagnetic of rGO and low loading of Ni. It is worth noting that the μ'' values are negative within a certain frequency range, which is similar to the result for many composites containing Ni as fillers [8,34]. Moreover, multiple resonance peaks are observed in the μ'' plots of composites with rGO/Ni ratio of 2:1 and 1:1, which can be assigned to natural resonance, eddy current and exchange resonance [35]. The above results suggest that the electromagnetic parameters of rGO/Ni composites can be easily controlled by the rGO proportion. Benefiting from the optimization design, the appropriate permittivity and permeability values of the corresponding composite can meet the requirement of impedance matching and thus make the incident microwave increased.

Impedance matching ratio as well as attenuation constant α are the two crucial factors in judging the electromagnetic property of sample. The former decides how much of microwave to propagate into materials; the latter determines the attenuation properties of materials which can be expressed as [36]:

$$\alpha = \frac{\sqrt{2}\pi f}{c} \times \sqrt{(\mu''\varepsilon'' - \mu'\varepsilon') + \sqrt{(\mu''\varepsilon'' - \mu'\varepsilon')^2 + (\mu'\varepsilon'' + \mu''\varepsilon')^2}} \quad (4)$$

where f and c are the frequency of the microwave and the velocity of light in a vacuum, respectively. As can be seen in Fig. 5, the impedance matching ratio of sample increases with the decreasing rGO/Ni mass ratio, which maximizes at 1:4. On the other hand, the attenuation constant of sample increases with increasing proportion of rGO, which is consistent with the result in permittivity (Fig. 4a and b). The sample with rGO/Ni ratio of 1:4 possesses the best impedance matching characteristic and worst attenuation ability because of its relatively low complex permittivity; contrarily, sample with rGO/Ni ratio of 4:1 owns the poorest impedance matching activity and superior attenuation property. Due to the impedance mismatching, the majority of incident electromagnetic wave may be reflected back on the sample surface, thus leading to a strong reflection. Meanwhile, if the attenuation capacity is weak, the penetrating wave cannot be completely attenuated. Considering the offset and balance between their impedance matching ratio and attenuation constant, it is deduced that the composites with rGO/Ni ratio of 2:1 and 1:1 may have the excellent microwave absorption performance.

To prove the above conclusion, the microwave absorption performance of rGO/Ni composites with different rGO proportions are evaluated by the reflection loss (RL) based on the basis of transmission line theory [16,37]:

$$RL = 20\log\left|\frac{Z_{in} - 1}{Z_{in} + 1}\right| \quad (5)$$

$$Z_{in} = \sqrt{\frac{\mu_r}{\varepsilon_r}}\tanh\left[j\left(\frac{2f\pi d}{c}\right)\sqrt{\mu_r\varepsilon_r}\right] \quad (6)$$

where Z_{in} is the normalized input characteristic impedance, ε_r and μ_r are the complex permittivity and permeability of the composite

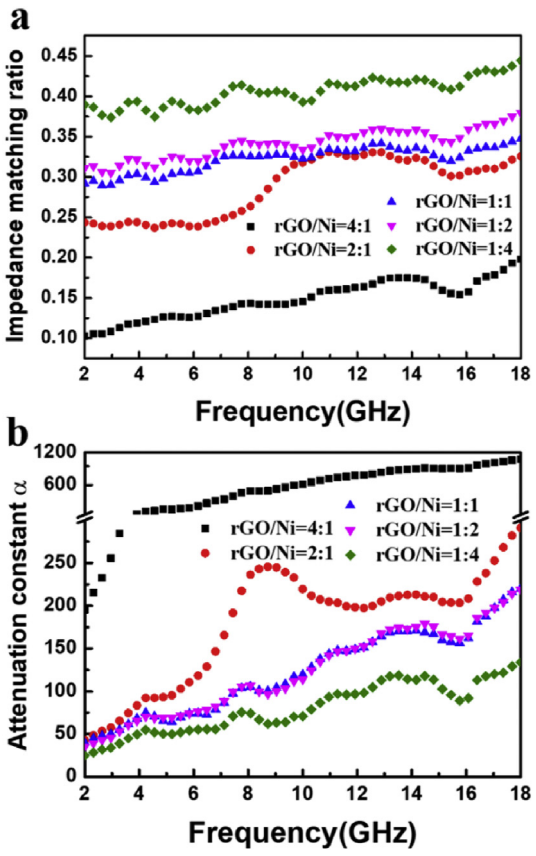

Fig. 5. Impedance matching ratio (a) and attenuation constant α (b) of rGO/Ni hybrids with different rGO proportions. (A colour version of this figure can be viewed online.)

absorber, respectively; d is the thickness of the absorber. When the RL is smaller than −10 dB, it is implied that more than 90% of the microwave is absorbed by materials, and the frequency range can be considered as effective absorption bandwidth. As observed in Fig. 6, at the beginning, with increasing of the rGO proportions, the microwave absorption performances of composite are significantly enhanced. An optimal RL value of −39.03 dB and a broad effective bandwidth of 4.3 GHz (11–15.3 GHz) are achieved for the composites with the rGO/Ni ratio of 1:1. Nevertheless, with the rGO proportion further increasing, the performances have been suppressed and become worse. This is caused by the unbalance between the sharp increase of permittivity and the stable fluctuation of permeability, thus leading to the impedance mismatch. Consequently, a highly efficient microwave absorbent with strong absorption ability and wide effective bandwidth has been demonstrated through regulating the electromagnetic parameters of composites.

The reflection loss of the composite with rGO/Ni ratio of 1:1 under different thickness is shown in Fig. 7a, and the 3D image map is shown in Fig. 7b. It is obvious that the RL peaks move to the lower frequency region as the thickness increased. Meanwhile, it is worth noting that the experimental results are in good agreement with the quarter wavelength (λ/4) matching model (Fig. 7c), the physical meaning is when the absorbent reaches the matching thickness (t_m) and satisfies the following equation (4), the reflected waves derived from the upper and bottom interface are out of phase by 180° and totally cancel each other in the air-absorbent interface [38,39]:

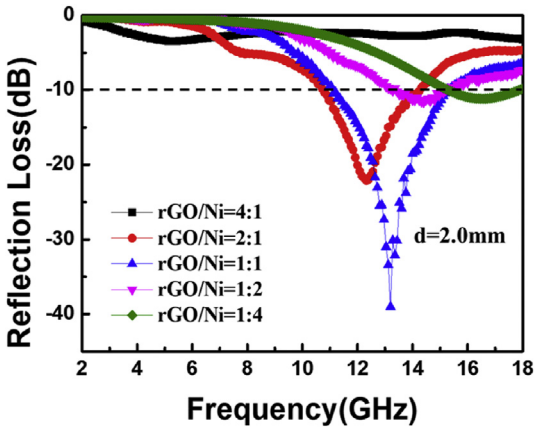

Fig. 6. Microwave RL curves of the rGO/Ni composites with different rGO proportions at a thickness of 2 mm in the frequency range of 2–18 GHz. (A colour version of this figure can be viewed online.)

$$t_m = \frac{n}{4}\lambda = \frac{nc}{4f_m|\sqrt{\mu_r\varepsilon_r}|}(n = 1,\ 3,\ 5) \tag{7}$$

Without a doubt, the quarter wavelength matching model are also well consistent with the contour map (Fig. 7d). Compared with the recently reports for the rGO-based materials, the rGO/Ni composite possesses superior microwave absorption ability at a rather thin thickness, which may be ascribed to the proper combination of the complex permittivity and permeability resulting in the appropriate synergistic effect of dielectric loss and magnetic loss. Besides, the special structure of the composite is fundamental to the enhancement of the absorption property. The chainlike morphology of nickel and the relatively large surface area of rGO can provide more active sites for multiple reflections and scattering, transforming the microwave energy to heat energy in long propagation periods (Fig. 8).

Furthermore, we attempted to investigate the electromagnetic interference (EMI) shielding effectiveness (*SE*) of the rGO/Ni composites. EMI shielding refers to the reflection and absorption of electromagnetic radiation by the material. The reflection coefficient *R*, transmission coefficient *T*, and absorption coefficient *A* are evaluated using *S*-parameters [40,41]: $T = |S_{12}|^2 = |S_{21}|^2$, $R = |S_{11}|^2 = |S_{22}|^2$, and $A = 1 - R - T$. The total EMI shielding effectiveness (SE_{total}) consists of the contributions from absorption loss (SE_A), reflection loss (SE_R), and multiple reflection (SE_M) [42,43]:

$$SE_{total}(dB) = SE_R + SE_A + SE_M \tag{8}$$

$$SE_R(dB) = 10log_{10}(1 - R) \tag{9}$$

$$SE_A(dB) = 10log_{10}[T/(1 - R)] \tag{10}$$

Usually SE_M is important only when composites are thin and are used at very low frequencies (i.e. ~kHz range). In our case, SE_M could be ignored because of the high measuring frequency and large distance between the reflecting surface and interface, compared to the skin depth. SE_{total} of materials can be calculated by using the scattering parameter as [44,45].

$$SE_{total}(dB) = 10 \times \log\left[\frac{1}{|s_{12}|^2}\right] = 10 \times \log\left[\frac{1}{|s_{21}|^2}\right] \tag{11}$$

The SE_{total} of the composites with the increasing rGO/Ni ratio in

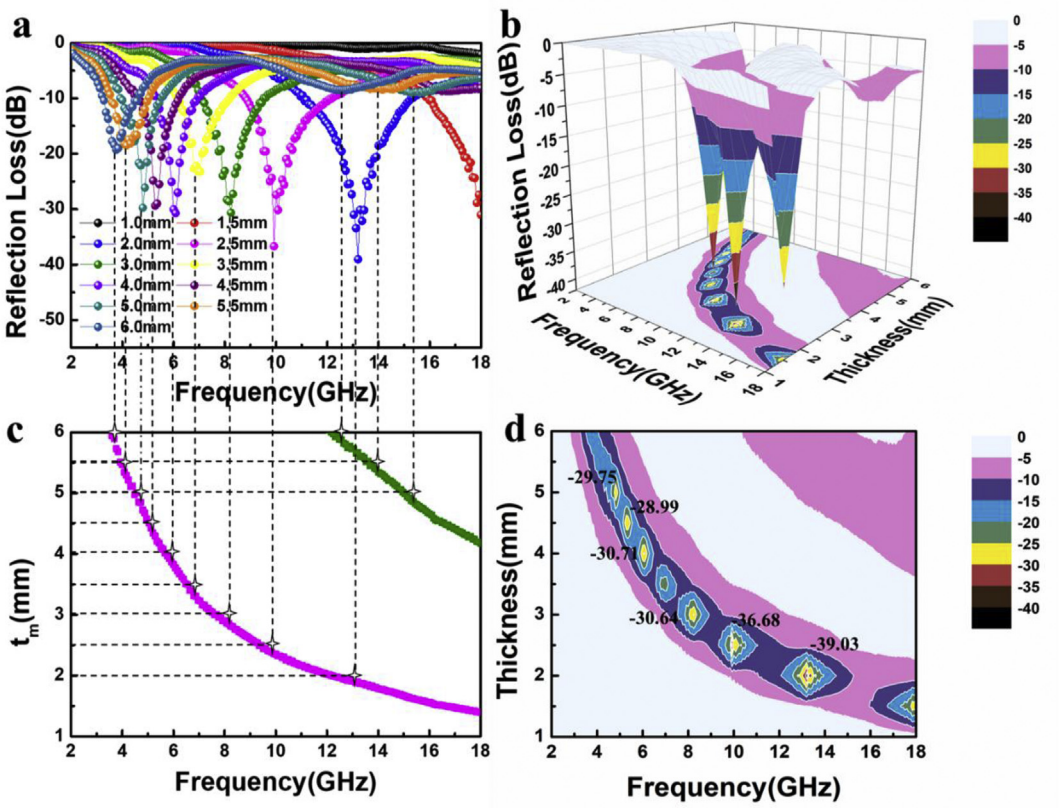

Fig. 7. Microwave RL curves (a), three-dimensional representation (b), the frequency dependence of matching thickness and calculated thickness t_m (c) and two-dimensional representation of the values of reflection loss (d) for rGO/Ni composites with rGO/Ni ratio of 1:1 under different thickness. (A colour version of this figure can be viewed online.)

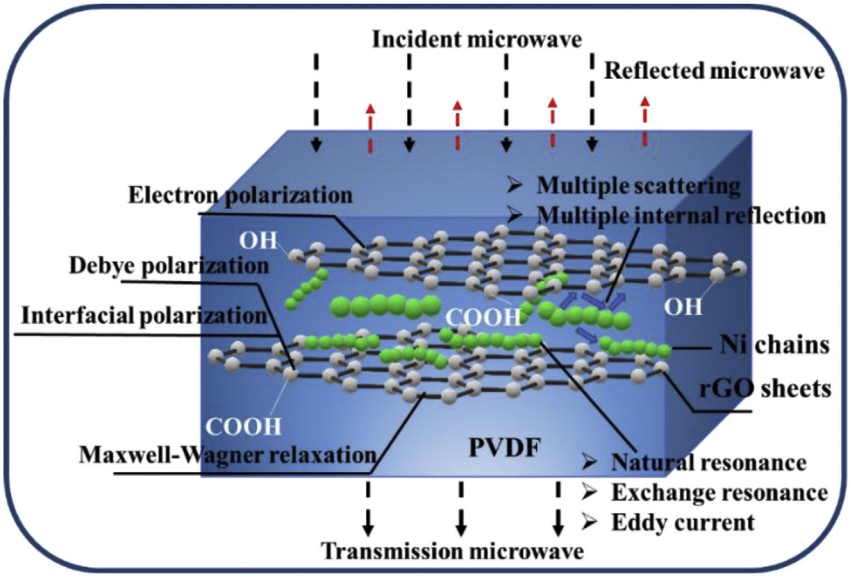

Fig. 8. Schematic of the possible microwave absorption mechanisms for the rGO/Ni composites. (A colour version of this figure can be viewed online.)

the frequency range of 2–18 GHz is shown in Fig. 9a, and the SE_R and SE_A are shown in Figure S4. It is clear that the lower impedance matching ratio would lead to higher reflection effectiveness and thus provide great contributions to EMI shielding. Besides, the ideal EMI shielding also involves strong absorption (SE_A) which could be easily altered based on the material thickness. From the sets of Fig. 9a, the SE_{total} values considerably increase with increasing mass ratio of the rGO over the entire frequency range. The composite with rGO/Ni ratio of 4:1 shows a great EMI SE value (>10 dB) at a thin thickness (~1 mm) but a poor absorption behavior as discussed in the previous paragraph. Generally, the pursuit of larger impedance mismatch and higher electric conductivity is an ideal strategy to achieve high-performance EMI shielding materials [46,47]. The excessive complex permittivity of the composites (4:1) indicating

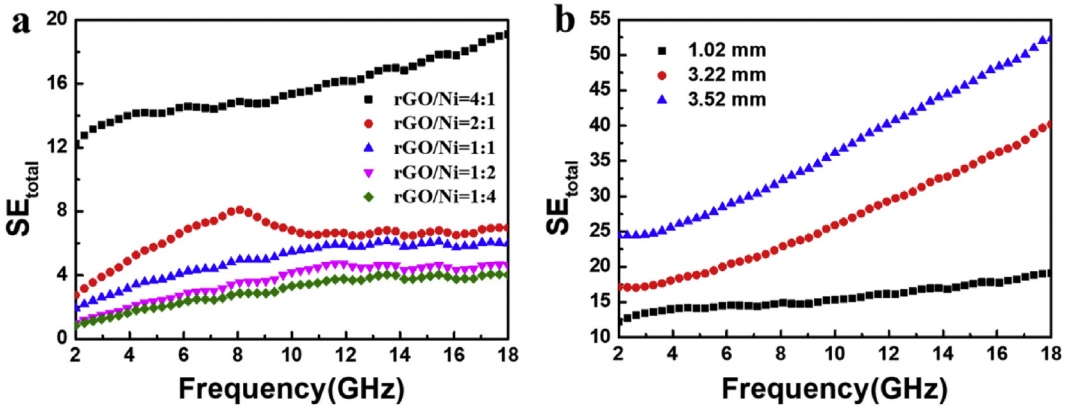

Fig. 9. (a) EMI shielding effectiveness as a function of frequency measured in the 8–12 GHz range of the rGO/Ni hybrids with various rGO/Ni concentrations; (b) EMI SE_{total} values of the hybrids with rGO/Ni of 4:1 at various film thicknesses. (A colour version of this figure can be viewed online.)

its potential EMI shielding ability, which is in consistent with the above results and discuss. To further enhance the EMI shielding effectiveness, we increase the thickness of the composites from 1.02 mm to 3.52 mm. As expected, the thicker composites show a much better EMI shielding effectiveness and more than 25 dB shielding effectiveness over the whole measuring frequency range is achieved (Fig. 9b).

Overall, the optimal EM absorption ability is attributed to the good impedance match, moderate conductivity, appropriate synergistic effect of dielectric loss and magnetic loss. On the other hand, for the EMI shielding materials, the required electrical conductivity could be much higher, while the larger impedance mismatch would block more EM waves for propagating into the materials. Therefore, above mechanisms and relationship as show in Fig. 10 should be considered, when we design and fabricate EM absorbing and EMI shielding materials.

4. Conclusion

In summary, the simple fabrication of magnetic and conductive rGO/Ni hybrids with different component proportion has been demonstrated. With good controllability of permittivity and permeability, the resultant composites exhibit excellent EM absorbing property together with considerable shielding performance. For composites with rGO/Ni ratio of 1:1, superior reflection loss of −39.03 dB is achieved at 13 GHz with a thickness of 2 mm. While rGO/Ni ratio up to 4:1, the EMI SE of composite is higher than 25 dB, and their effective bandwidths (SE > 20 dB) covers the whole measured frequency totally. The aforementioned results provide a strategy that can be widely applied in many fields, presenting great opportunities for designing and fabricating advanced electromagnetic absorbing and shielding materials.

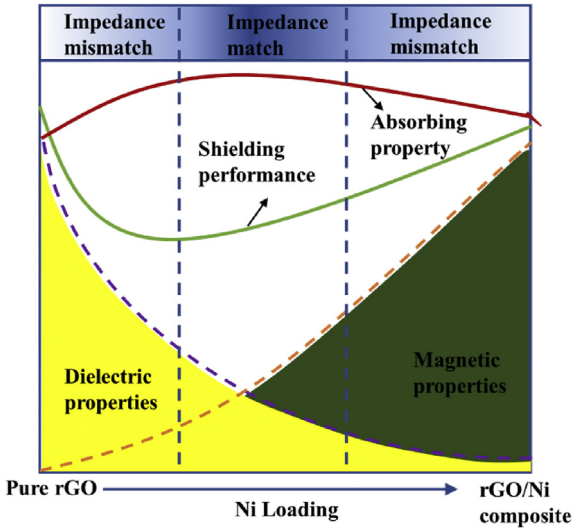

Fig. 10. Scheme of the absorbing and shielding performance: relationship with the changes in both dielectric and magnetic properties. (A colour version of this figure can be viewed online.)

Acknowledgements

This project was supported by the National Nature Science Foundation of China (No.51472012) and the Fundamental Research Funds for the Central Universities.

Appendix A. Supplementary data

Supplementary data related to this article can be found at https://doi.org/10.1016/j.carbon.2018.07.044.

References

[1] B. Zhao, W.Y. Zhao, G. Shao, B.B. Fan, R. Zhang, Morphology-control synthesis of a core-shell structured NiCu alloy with tunable electromagnetic-wave absorption capabilities, ACS Appl. Mater. Interfaces 7 (23) (2015) 12951–12960.
[2] R. Dhawan, Kumari Saroj, R. Kumar, S.K. Dhawanb, S.R. Dhakate, Mesocarbon microsphere composites with Fe_3O_4 nanoparticles for outstanding electromagnetic interference shielding effectiveness, RSC Adv. 5 (54) (2015) 43279–43289.
[3] H. Lv, X. Liang, Y. Cheng, H. Zhang, D. Tang, B. Zhang, et al., Coin-like α-Fe_2O_3@$CoFe_2O_4$ core–shell composites with excellent electromagnetic absorption performance, ACS Appl. Mater. Interfaces 7 (8) (2015) 4744–4750.
[4] J. Xiang, J. Li, X. Zhang, Q. Ye, J. Xu, X. Shen, Magnetic carbon nanofibers containing uniformly dispersed Fe/Co/Ni nanoparticles as stable and high-performance electromagnetic wave absorbers, J. Mater. Chem. A 2 (40) (2014) 16905–16914.
[5] Y. Wang, L. Wang, H. Wu, Enhanced microwave absorption properties of α-Fe_2O_3-Filled ordered mesoporous carbon nanorods, Materials 6 (4) (2013) 1520–1529.
[6] T. Wu, Y. Liu, X. Zeng, T.T. Cui, Y.T. Zhao, Y.N. Li, et al., Facile hydrothermal synthesis of Fe_3O_4/C core-shell nanorings for efficient low-frequency microwave absorption, ACS Appl. Mater. Interfaces 8 (11) (2016) 7370–7380.
[7] Z. Wang, L. Wu, J. Zhou, W. Cai, B. Shen, Z. Jiang, Magnetite nanocrystals on multiwalled carbon nanotubes as a synergistic microwave absorber, ACS Appl. Mater. Interfaces 117 (10) (2013) 5446–5452.
[8] F. Wen, F. Zhang, Z. Liu, Investigation on microwave absorption properties for multiwalled carbon nanotubes/Fe/Co/Ni nanopowders as lightweight absorbers, J. Phys. Chem. C 115 (29) (2011) 14025–14030.
[9] F. Wen, H. Hou, J. Xiang, X. Zhang, Z. Su, S. Yuan, et al., Fabrication of carbon encapsulated Co_3O_4 nanoparticles embedded in porous graphitic carbon nanosheets for microwave absorber, Carbon 89 (2015) 372–377.

[10] B. Zhao, X.Q. Guo, W.Y. Zhao, J.S. Deng, G. Shao, B.B. Fan, et al., Yolk-shell Ni@SnO_2 composites with a designable interspace to improve electromagnetic wave absorption properties, ACS Appl. Mater. Interfaces 8 (42) (2016) 28917–28925.
[11] H.J. Yang, W.Q. Cao, D.Q. Zhang, T.J. Su, H.L. Shi, W.Z. Wang, et al., NiO hierarchical nanorings on SiC: enhancing relaxation to tune microwave absorption at elevated temperature, ACS Appl. Mater. Interfaces 7 (13) (2015) 7073–7077.
[12] J. Liu, J. Cheng, R. Che, J. Xu, M. Liu, Z. Liu, Synthesis and microwave absorption properties of yolk–shell microspheres with magnetic iron oxide cores and hierarchical copper silicate shells, ACS Appl. Mater. Interfaces 5 (7) (2013) 2503–2509.
[13] Q.H. Liu, Q. Cao, H. Bi, C.Y. Liang, K.P. Yuan, W. She, et al., CoNi@SiO_2@TiO_2 and CoNi@Air@TiO_2 microspheres with strong wideband microwave absorption, Adv. Mater. 28 (3) (2015) 486–490.
[14] C. Zhang, B. Wang, J. Xiang, C. Su, C. Mu, F. Wen, et al., Microwave absorption properties of CoS_2 nanocrystals embedded into reduced graphene oxide, ACS Appl. Mater. Interfaces 9 (34) (2017) 28868–28875.
[15] Y. Wang, D. Chen, X. Yin, P. Xu, F. Wu, M. He, Hybrid of MoS_2 and reduced graphene oxide: a lightweight and broadband electromagnetic wave absorber, ACS Appl. Mater. Interfaces 7 (47) (2015) 26226–26234.
[16] R.C. Che, L.M. Peng, X.F. Duan, Q. Chen, X.L. Liang, Microwave absorption enhancement and complex permittivity and permeability of Fe encapsulated within carbon nanotubes, Adv. Mater. 16 (5) (2004) 401–405.
[17] J. Ran, L. Shen, L. Zhong, H. Fu, Synthesis of silanized MoS_2/reduced graphene oxide for strong radar wave absorption, Ind. Eng. Chem. Res. 56 (38) (2017) 10667–10677.
[18] A.P. Guo, X.J. Zhang, S.W. Wang, J.Q. Zhu, L. Yang, G.S. Wang, Excellent microwave absorption and electromagnetic interference shielding based on reduced graphene oxide@MoS_2/poly(vinylidene fluoride) composites, ChemPlusChem 81 (2016) 1305–1311.
[19] S. Kim, J.S. Oh, M.G. Kim, W. Jang, M. Wang, Y. Kim, et al., Electromagnetic interference (EMI) transparent shielding of reduced graphene oxide (RGO) interleaved structure fabricated by electrophoretic deposition, ACS Appl. Mater. Interfaces 6 (20) (2014) 17647–17653.
[20] D.X. Yan, H. Pang, B. Li, R. Vajtai, L. Xu, P.G. Ren, et al., Structured reduced graphene oxide/polymer composites for ultra-efficient electromagnetic interference shielding, Adv. Funct. Mater. 25 (4) (2015) 559–566.
[21] W.L. Song, C. Gong, H. Li, X.D. Cheng, M. Chen, X. Yuan, et al., Graphene-based sandwich structures for frequency selectable electromagnetic shielding, ACS Appl. Mater. Interfaces 9 (41) (2017) 36119–36129.
[22] X. Jian, B. Wu, Y.F. Wei, S.X. Dou, X.L. Wang, W.D. He, et al., Facile synthesis of Fe_3O_4/GCs composites and their enhanced microwave absorption properties, ACS Appl. Mater. Interfaces 8 (9) (2016), 6101–9.
[23] M. Zong, Y. Huang, Y. Zhao, X. Sun, C. Qu, D. Luo, et al., Facile preparation, high microwave absorption and microwave absorbing mechanism of rGO-Fe_3O_4 composites, RSC Adv. 3 (45) (2013) 23638–23648.
[24] M. Mishra, A.P. Singh, B.P. Singh, V.N. Singhc, S.K. Dhawan, Conducting ferrofluid: a high-performance microwave shielding material, J. Mater. Chem. A 2 (32) (2014) 13159–13168.
[25] K. Singh, A. Ohlan, V.H. Pham, R. Balasubramaniyan, S. Varshney, J. Jang, et al., Nanostructured graphene/Fe_3O_4 incorporated polyaniline as a high-performance shield against electromagnetic pollution, Nanoscale 5 (6) (2013) 2411–2420.
[26] L. Kong, X. Yin, Y. Zhang, X. Yuan, Q. Li, F. Ye, et al., Electromagnetic wave absorption properties of reduced graphene oxide modified by maghemite colloidal nanoparticle clusters, J. Phys. Chem. C 117 (38) (2013), 19701–11.
[27] X. Liang, B. Quan, G. Ji, W. Liu, H. Zhao, S. Dai, et al., Tunable dielectric performance derived from the metal–organic framework/reduced graphene oxide hybrid with broadband absorption, ACS Sustain. Chem. Eng. 5 (11) (2017) 10570–10579.
[28] W. Xu, Y.F. Pan, W. Wei, G.S. Wang, P. Qu, Microwave absorption enhancement and dual-nonlinear magnetic resonance of ultra small nickel with quasi-one-dimensional nanostructure, Appl. Surf. Sci. 428 (2018) 54–60.
[29] H. Pan, M. Xu, Q. Qi, X. Liu, Facile preparation and excellent microwave absorption properties of an RGO@$Co_{0.33}Ni_{0.67}$ lightweight absorber, RSC Adv. 7 (69) (2017) 43831–43838.
[30] X.J. Zhang, G.S. Wang, W.Q. Cao, Y.Z. Wei, J.F. Liang, L. Guo, et al., Enhanced microwave absorption property of reduced graphene oxide (RGO)-$MnFe_2O_4$ nanocomposites and polyvinylidene fluoride, ACS Appl. Mater. Interfaces 6 (10) (2014) 7471–7478.
[31] B. Wen, X.X. Wang, W.Q. Cao, H.L. Shi, M.M. Lu, G. Wang, et al., Reduced graphene oxides: the thinnest and most lightweight materials with highly efficient microwave attenuation performances of the carbon world, Nanoscale 6 (11) (2014) 5754–5761.
[32] M.S. Cao, C. Han, X.X. Wang, M. Zhang, Y.L. Zhang, J.C. Shu, et al., Graphene nanohybrids: excellent electromagnetic properties for the absorbing and shielding of electromagnetic waves, J. Mater. Chem. C 6 (17) (2018) 4586–4602.
[33] H.B. Zhao, Z.B. Fu, H.B. Chen, M.L. Zhong, C.Y. Wang, Excellent electromagnetic absorption capability of Ni/Carbon based conductive and magnetic foams synthesized via a green one pot route, ACS Appl. Mater. Interfaces 8 (2) (2016) 1468–1477.
[34] B. Zhao, C.B. Park, Tunable electromagnetic shielding properties of conductive poly(vinylidene fluoride)/Ni chain composite films with negative permittivity, J. Mater. Chem. C 5 (28) (2017) 6954–6961.
[35] G.Z. Wang, Z. Gao, G.P. Wan, S.W. Lin, P. Yang, Y. Qin, High densities of magnetic nanoparticles supported on graphene fabricated by atomic layer deposition and their use as efficient synergistic microwave absorbers, Nano Res. 7 (5) (2014) 704–716.
[36] X.G. Liu, Z.Q. Qu, D.Y. Geng, Z. Han, J.J. Jiang, W. Liu, et al., Influence of a graphite shell on the thermal and electromagnetic characteristics of FeNi nanoparticles, Carbon 48 (3) (2010) 891–897.
[37] M.S. Cao, W.L. Song, Z.L. Hou, B. Wen, J. Yuan, The effects of temperature and frequency on the dielectric properties, electromagnetic interference shielding and microwave absorption of short carbon fiber/silica composites, Carbon 48 (3) (2010) 788–796.
[38] R. Yang, B. Wang, J. Xiang, C. Mu, C. Zhang, F. Wen, et al., Fabrication of $NiCo_2$-anchored graphene nanosheets by liquid-phase exfoliation for excellent microwave absorbers, ACS Appl. Mater. Interfaces 9 (14) (2017) 12673–12679.
[39] B. Wang, J. Wei, Y. Yang, T. Wang, F. Li, Investigation on peak frequency of the microwave absorption for carbonyl iron/epoxy resin composite, J. Magn. Magn Mater. 323 (8) (2011) 1101–1103.
[40] Y. Chen, H.B. Zhang, Y.B. Yang, M. Wang, A.Y. Cao, Z.Z. Yu, High-performance epoxy nanocomposites reinforced with three-dimensional carbon canotube sponge for electromagnetic interference shielding, Adv. Funct. Mater. 26 (3) (2016) 447–455.
[41] Z. Zeng, H. Jin, M. Chen, W. Li, L. Zhou, Z. Zhang, Lightweight and anisotropic porous MWCNT/WPU composites for ultrahigh performance electromagnetic interference shielding, Adv. Funct. Mater. 26 (2) (2016) 303–310.
[42] W.L. Song, J. Wang, L.Z. Fan, Y. Li, C.Y. Wang, M.S. Cao, Interfacial engineering of carbon nanofiber-graphene-carbon nanofiber heterojunctions in flexible lightweight electromagnetic shielding networks, ACS Appl. Mater. Interfaces 6 (13) (2014) 10516–10523.
[43] W.L. Song, M.S. Cao, L.Z. Fan, M.M. Lu, Y. Li, C.Y. Wang, H.F. Ju, Highly ordered porous carbon/wax composites for effective electromagnetic attenuation and shielding, Carbon 77 (10) (2014) 130–142.
[44] S. Kim, J.S. Oh, M.G. Kim, W. Jang, M. Wang, Y. Kim, H.W. Seo, Y.C. Kim, J.H. Lee, Y. Lee, J.D. Nam, Electromagnetic interference (EMI) transparent shielding of reduced graphene oxide (RGO) interleaved structure fabricated by electrophoretic deposition, ACS Appl. Mater. Interfaces 6 (20) (2014) 17647–17653.
[45] P.K. Mural, S.P. Pawar, S. Jayanthi, G. Madras, A.K. Sood, S. Bose, Engineering nanostructures by decorating magnetic nanoparticles onto graphene oxide sheets to shield electromagnetic radiations, ACS Appl. Mater. Interfaces 7 (30) (2015) 16266–16278.
[46] Q. Song, F. Ye, X. Yin, W. Li, H. Li, Y. Liu, et al., Carbon nanotube-multilayered graphene edge plane core-shell hybrid foams for ultrahigh-performance electromagnetic-interference shielding, Adv. Mater. 29 (31) (2017), 1701583.
[47] Z. Zeng, H. Jin, M. Chen, W. Li, L. Zhou, X. Xue, et al., Microstructure design of lightweight, flexible, and high electromagnetic shielding porous multiwalled carbon nanotube/polymer composites, Small 13 (34) (2017), 1701388.